

Crystal growth, optical and spectroscopic characterisation of monoclinic $\text{KY}(\text{WO}_4)_2$ co-doped with Er^{3+} and Yb^{3+}

X. Mateos, R. Solé, Jna. Gavaldà, M. Aguiló, J. Massons, F. Díaz *

Física i Cristal·lografia de Materials (FiCMA), Universitat Rovira i Virgili, Campus Sescelades C/Marcel·lí Domingo, s/n. 43007 Tarragona, Spain

Received 5 May 2004; accepted 30 December 2004

Available online 20 June 2005

Abstract

We grew un-doped $\text{KY}(\text{WO}_4)_2$ (hereafter KYW), Er^{3+} and Yb^{3+} single-doped KYW and Er^{3+} , Yb^{3+} co-doped KYW single crystals at several dopant concentrations by the Top-Seeded Solution Growth slow-cooling method (TSSG). We studied several optical properties of the host (the transparency window, the orientation of the principal optical axes and the measurement of the refractive indices as a function of the wavelength). We also analysed the spectroscopy of Er^{3+} and Yb^{3+} ions in KYW in terms of the optical absorption at room temperature (RT) and at low temperature (6 K), and the luminescence at RT and 10 K in the 1425–1650 nm range corresponding to the 1.5 μm emission of Er^{3+} ($^4\text{I}_{13/2} \rightarrow ^4\text{I}_{15/2}$ transition), after pumping at 981 nm (overlap in energy between $^4\text{I}_{11/2}$ and $^2\text{F}_{5/2}$ levels of Er^{3+} and Yb^{3+} , respectively) and at 798 nm ($^4\text{I}_{9/2}$ level of Er^{3+}). Luminescence was studied in terms of optical emission and lifetimes measurements.

© 2005 Elsevier B.V. All rights reserved.

PACS: 81.10.Dn; 42.70.Hj; 78.55.-m

Keywords: Erbium; Ytterbium; $\text{KY}(\text{WO}_4)_2$; Infrared emission

1. Introduction

In the past few years, rare-earth ions, specially erbium, have played an important role in the development of optical communication technology. Trivalent erbium has an incomplete 4f electronic shell that is shielded by the 5s and 5p shells. As a result, rather sharp optical intra-4f transitions can be achieved from erbium-doped materials. The transition from the first excited state to the ground state in Er^{3+} occurs around an energy of 6500 cm^{-1} , which corresponds to a wavelength of 1.5 μm . This is an important telecommunication wavelength because standard silica-based optical fibers have their maximum transparency at this wavelength.

The main disadvantage of Er^{3+} is its low absorption cross-section in the laser diodes emission range (0.8–1.5 μm), which limits pump efficiency. A possible improvement involves co-doping the material with a second ion that acts as a sensitizer of the active ion. Ytterbium is the ideal candidate for this role, not only because of its high absorption cross-section but also because of the broad absorption band that offers excitation tuning in the 920–1000 nm wavelength region and the large overlap between ytterbium emission and erbium absorption, which allows resonant energy transfer from Yb to Er.

The low-temperature monoclinic phase of potassium rare-earth tungstates (KREW) can be doped with optical active lanthanide ions, even at a high-concentration level, to constitute solid-state laser materials. The KYW crystal has a monoclinic crystallographic structure with space group $C2/c$ and lattice parameters

* Corresponding author. Tel.: +34 977559517; fax: +34 977559563.
E-mail address: diaz@quimica.urv.es (F. Díaz).

$a = 10.64 \text{ \AA}$, $b = 10.35 \text{ \AA}$, $c = 7.54 \text{ \AA}$ and $\beta = 130.5(2)^\circ$ [1].

In this paper we present the crystal growth of un-doped KYW, Er and Yb single-doped KYW and Er, Yb co-doped KYW single crystals at several dopant concentrations. We study several of the host's optical properties, as well as the spectroscopic properties of Er sensitised by Yb. For the optical properties of the host, we studied the transparency window, the orientation of the principal optical axes and measured the refractive indices as a function of the wavelength. For the spectroscopic properties, we studied optical absorption (at RT and 6 K), optical emission of the 1.5 μm emission (at RT and 10 K) and lifetime measurements at RT. The emissions were studied in the 1425–1630 nm range under 981 and 798 nm pump excitation.

2. Experiment

We grew the crystals by the Top-Seeded Solution Growth slow-cooling method (TSSG) and chose $\text{K}_2\text{W}_2\text{O}_7$ as solvent because it eliminates the possible introduction of foreign components into the solution. It also has a relatively low-melting temperature (892 K) [2] and its content tungsten is higher than that of the K_2WO_4 solvent, which is also used to grow KREW crystals [3]. This minimises the viscosity of the solution and enables the crystal to grow at relatively low temperatures and low viscosity. Previous studies have shown that $\text{K}_2\text{W}_2\text{O}_7$ is a promising high-temperature solvent for growing doped KREW crystals because the concentration and temperature ranges of crystallisation of the low-temperature phase (which has a monoclinic structure) are sufficiently wide, [4] the solubility of the components at temperatures of the order of 1273 K is good, homogenisation of the solutions is easy, volatility is low and the tendency to creep is negligible. Other crystal growth methods are suitable for KREW crystals like the top nucleated floating crystal method, used in Ref. [5].

We grew the crystals with a binary solution composition of 11.5 mol% solute/88.5 mol% solvent. To obtain the monoclinic phase, we used platinum crucibles 50 mm in diameter to prepare around 200 g of solution, and decomposed the appropriate quantities of K_2CO_3 , Y_2O_3 , and WO_3 for un-doped KYW crystals and Er_2O_3 and Yb_2O_3 for Er, Yb-doped crystals (Fluka, 99.9% pure), in accordance with the composition of the crystals. We used a b -oriented piece of KYW single crystal as a seed for crystal growth because previous studies [6] of $\text{KGdW}:\text{Ln}^{3+}$ crystal growth showed that with this orientation the crystals grow faster than with other crystallographic orientations and produce inclusion-free crystals.

We used a vertical tubular furnace with Kanthal heating elements. The furnace was equipped with a temperature controller and a programmer as well as control thermocouples.

The composition of the crystals was determined by Electron-Probe Microanalysis (EPMA) with Cameca SX 50 equipment.

To prepare the samples for the optical and spectroscopic studies, we cut the crystals using a goniometer and a Struers Accutom-50 diamond saw and polished them with a Logytech PM5 polisher with an oscillatory arm that allowed us to accurately rotate and pressurise the samples depending on the hardness of the material.

We measured the transparency window of un-doped KYW sample with a VARIAN CARY-5E-UV-VIS-NIR 500Scan Spectrophotometer in Transmission mode.

The low-temperature phase of KYW belongs to the $2/m$ crystallographic point group. It is therefore a biaxial crystal with inversion centre. The three orthogonal principal optical axes are labelled N_g , N_m and N_p . These correspond to the directions with maximum, medium and minimum values of refractive index (n_g , n_m and n_p), respectively. In monoclinic crystals, one of the principal axes (in this case N_p) is always parallel to the C_2 symmetry axis. This coincides with the crystallographic b axis, so the other two principal axes (in this case, N_g and N_m) lie in the a – c plane because the b axis is orthogonal to this plane. By determining the angle between the c axis and the N_g (or N_m) principal axis in the a – c plane, we locate the orientation of the optical indicatrix of KYW. The experimental set-up for determining the optical indicatrix comprised two crossed polarisers that ensure the minimum transmission of light. We put the sample between them and at the same time moved the polarisers to again find the minimum transmission of light. To do this, we fixed the sample but connected the polarisers using an oscillatory arm. The deviated angle corresponded to the angle between a principal optical direction and a crystallographic axis.

We performed the optical absorption of KYW:Er, KYW:Yb crystals along b direction and the polarised optical absorption of KYW:Er, Yb crystals at RT and 6 K. The latter was made with light parallel to the three principal optical directions. The composition of the crystals was 1.64×10^{20} at./cm³ of erbium for KYW:Er, 7.09×10^{19} at./cm³ of ytterbium for KYW:Yb, and 3.15×10^{19} and 2.40×10^{20} at./cm³ of erbium and ytterbium, respectively, for KYW:Er, Yb crystals. The thickness of the samples was 240 μm for KYW:Er, 610 μm for KYW:Yb and 480 μm for KYW:Er, Yb ($E \parallel N_g$ and $E \parallel N_m$) and 1.97 mm for KYW:Er, Yb ($E \parallel N_p$). The measurements were taken with the same spectrophotometer as the one used for transmission experiments, and a Glan-Taylor polariser. Cryogenic temperatures were obtained with a Leybold cycle helium RDK 6-320 cryostat.

The equipment for our photoluminescence experiments comprised a BMI Optical Parametric Oscillator (OPO) pumped by the third harmonic of a seeded BMI SAGA YAG:Nd laser. Pulses of 15 mJ were achieved with a Gaussian beam profile. Fluorescence was dispersed through a Jobin Yvon-Spex monochromator HR460 model. We used a cooled Hamamatsu NIR R5509-72 photomultiplier. The luminescence signal was analysed by a EG&G 7265DSP lock-in amplifier and cryogenic temperatures were obtained by an Oxford closed-cycle helium CCC1104 cryostat. The emission spectra were performed at RT and 10 K on the same samples as those used for optical absorption studies and were corrected by the spectral response of the photomultiplier which was reasonably flat in the analysed spectral range.

Lifetime measurements were taken with the averaging facilities of a computer-controlled Tektronix TDS-714 digital oscilloscope.

3. Results and discussion

3.1. Crystal growth and composition of crystals

We grew un-doped potassium yttrium tungstate single crystals (KYW). We also grew single-doped erbium and ytterbium, $KY_{1-x}Er_x(WO_4)_2$ and $KY_{1-y}Yb_y(WO_4)_2$, and co-doped erbium and ytterbium $KY_{1-x-y}Er_xYb_y(WO_4)_2$ single crystals. The crystals were doped at several concentrations. The temperature gradient in the solution was 0.2 K/mm and the saturation temperature was between 1164 and 1170 K. The crystal growth experiments were carried out along the **b** crystallographic orientation. The cooling interval

was 2 K at a cooling rate of 0.1 K h⁻¹ and 10 K at a cooling rate of 0.05 K h⁻¹. The crystals weighed 2.6–4.3 g, and the dimensions were 10–19 mm along the **c** crystallographic direction, 6–11 mm along the **a*** direction and 7–10 mm along the **b** direction. The single crystals presented no inclusions or macrodefects. A distribution coefficient close to unity means that the solution composition is conserved in the crystal. This allows us to obtain single crystals with a high-compositional homogeneity. In the case of the Yb³⁺ ion, this was not strictly true. Table 1 shows the EPMA results and Fig. 1 shows a photograph of a KYW:Er,Yb single crystal.

3.2. Optical characterisation of the host

We measured the optical transmission of a 0.2 mm thick KYW crystal along **b** direction in the 0.3–10 μm range. The UV cut-off wavelength was 315 nm and the clear transparency for this thickness extended from 350 nm to 5400 nm. Fig. 2 shows these results.

We used a cube cut with its faces perpendicular to the three principal axes and determined that the principal optical axis with maximum refractive index, N_g , was at 18.5 °C with respect to the **c** axis in the clock-wise rotation with the **b** axis pointing towards the observer. Fig. 3 shows the orientation of the principal optical axes with respect to the crystallographic axes.

We measured the refractive indices along the principal optical directions. This was measured between 0.45 and 1.5 μm by the minimum deviation angle method with two semi-prisms, which is described in more detail in [7]. The semi-prisms were cut in different principal planes to obtain n_g , n_m and n_p (one of these was obtained twice). To vary the excitation wavelength, we used the same OPO-laser system as that for luminescence

Table 1
Distribution coefficients and dopant concentrations measured by EPMA

% Sol Er	% Sol Yb	K_{Er}	K_{Yb}	[Er] (cm ⁻³)	[Yb] (cm ⁻³)	Stoichiometric formula
0.5	0.5			–	–	KY _{0.994} Er _{0.006} Yb _{0.000} (WO ₄) ₂
0.5	1.5	1.14	0.70	3.78 × 10 ¹⁹	6.31 × 10 ¹⁹	KY _{0.984} Er _{0.006} Yb _{0.010} (WO ₄) ₂
0.5	2.5	0.97	0.72	3.78 × 10 ¹⁹	1.14 × 10 ²⁰	KY _{0.977} Er _{0.005} Yb _{0.018} (WO ₄) ₂
0.5	5	0.88	0.75	3.15 × 10 ¹⁹	2.40 × 10 ²⁰	KY _{0.958} Er _{0.004} Yb _{0.038} (WO ₄) ₂
1.5	1.5	1.07	0.52	1.01 × 10 ²⁰	5.05 × 10 ¹⁹	KY _{0.976} Er _{0.016} Yb _{0.008} (WO ₄) ₂
1.5	2.5	1.01	0.67	9.46 × 10 ¹⁹	1.01 × 10 ²⁰	KY _{0.969} Er _{0.015} Yb _{0.016} (WO ₄) ₂
1.5	5	1.00	0.87	9.46 × 10 ¹⁹	2.71 × 10 ²⁰	KY _{0.946} Er _{0.015} Yb _{0.043} (WO ₄) ₂
1.5	7.5	0.97	0.92	9.46 × 10 ¹⁹	4.35 × 10 ²⁰	KY _{0.916} Er _{0.015} Yb _{0.069} (WO ₄) ₂
2.5	2.5	1.09	0.71	1.70 × 10 ²⁰	1.14 × 10 ²⁰	KY _{0.955} Er _{0.027} Yb _{0.018} (WO ₄) ₂
2.5	5	0.99	0.67	1.58 × 10 ²⁰	2.14 × 10 ²⁰	KY _{0.942} Er _{0.025} Yb _{0.034} (WO ₄) ₂
2.5	7.5	1.05	0.794	1.64 × 10 ²⁰	3.78 × 10 ²⁰	KY _{0.914} Er _{0.026} Yb _{0.060} (WO ₄) ₂
2.5	10	1.08	0.94	1.70 × 10 ²⁰	5.93 × 10 ²⁰	KY _{0.879} Er _{0.027} Yb _{0.094} (WO ₄) ₂

K_{Ln} denotes the distribution coefficient of the dopant in the host, calculated from the formulae below:

$$\text{Coefficient of distribution of } Er^{3+} \text{ in the crystal, } K_{Er^{3+}} = \frac{(\text{moles } Er^{3+} / (\text{moles } Yb^{3+} + \text{moles } Er^{3+}))_{\text{crystal}}}{(\text{moles } Er^{3+} / (\text{moles } Yb^{3+} + \text{moles } Er^{3+}))_{\text{solution}}}$$

$$\text{Coefficient of distribution of } Yb^{3+} \text{ in the crystal, } K_{Yb^{3+}} = \frac{(\text{moles } Yb^{3+} / (\text{moles } Yb^{3+} + \text{moles } Er^{3+}))_{\text{crystal}}}{(\text{moles } Yb^{3+} / (\text{moles } Yb^{3+} + \text{moles } Er^{3+}))_{\text{solution}}}$$

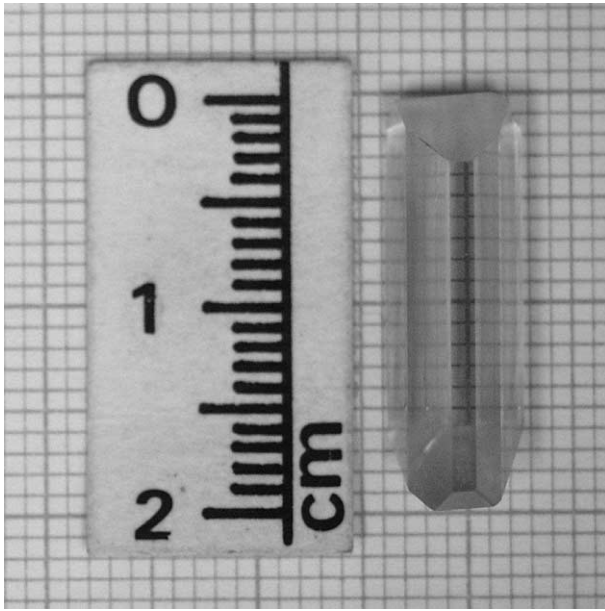


Fig. 1. Photograph of a KYW:Er,Yb single crystal grown by the TSSG slow cooling method.

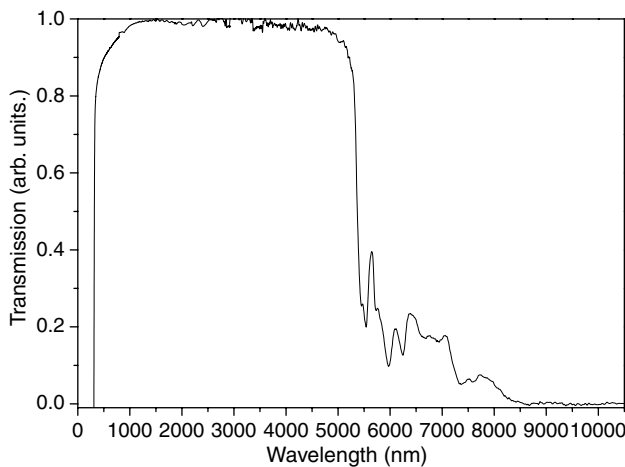


Fig. 2. Transparency window of a 0.2 mm thick plate of KYW in the 0.3–10 μm .

experiments. The dispersive chromatic curves are shown in Fig. 4. The values agree with the values provided by Kaminskii et al. [8]. The refractive indices of KYW are very similar to those of KGW [9] but lower than those of KYbW [10] and KLuW [11]. Table 2 summarises Sellmeier coefficients for these curves.

3.3. Spectroscopic characterisation of Er^{3+} and Yb^{3+} ions

3.3.1. Optical absorption

Fig. 5 shows the absorption of KYW:Er and KYW:Yb crystals in the 900–1000 nm range at 6 K to visualize the energy overlap between the $^4\text{I}_{11/2}$ level of erbium

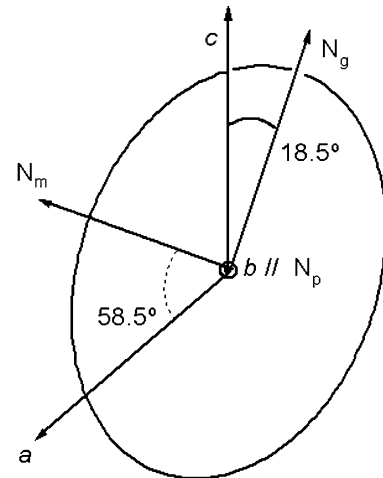


Fig. 3. Orientation of the principal optical axes versus the crystallographic axes in KYW crystals.

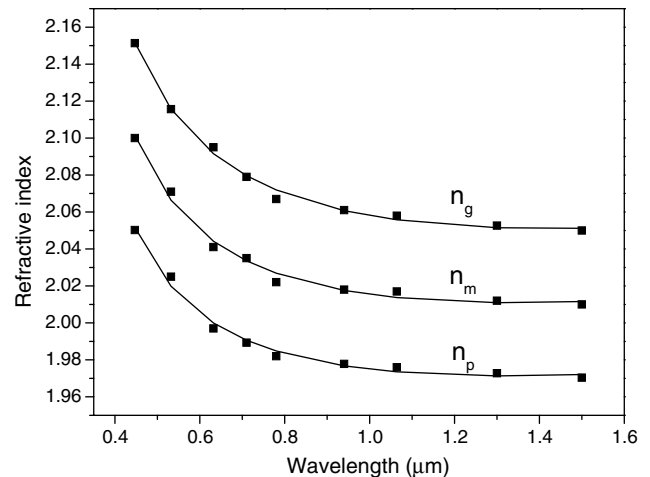


Fig. 4. Dispersive chromatic curves of KYW from 450 to 1500 nm.

Table 2

Room-temperature Sellmeier coefficients of KYW

Principal refractive index	A	B	C (μm)	D (μm^{-2})
n_g	3.55544	0.46438	0.15213	-0.03408
n_m	3.57271	0.30991	0.17484	-0.03401
n_p	3.50441	0.24431	0.18268	-0.03022

and the $^2\text{F}_{5/2}$ of ytterbium, and determine the energy position of the Stark levels of these two levels. We rescaled the intensities to show the two spectra clearly. The energy values of the Stark levels are summarised in Table 3 which are slightly different to those published by Macalik et al. [12]. The inset in Fig. 5 shows the polarised optical absorption cross-section of KYW:Yb,Er in the 875–1050 nm range at RT. Note the high anisotropy induced by the host. The maximum absorption cross-section was about $11.7 \times 10^{-20} \text{ cm}^2$ at 980.6 nm

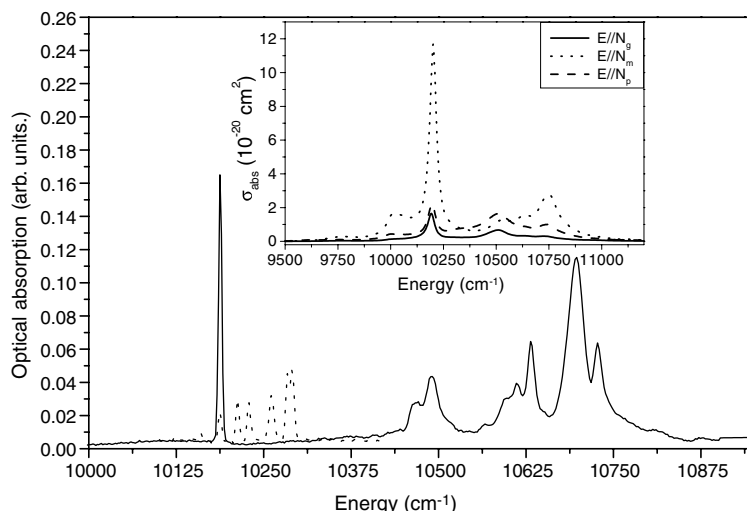


Fig. 5. Optical absorption of KYW:Yb (solid line) and KYW:Er (dotted line) in the 900–1000 nm range at 6 K. Inset: Polarised optical absorption in the 875–1050 nm of KYW:Er,Yb at RT.

Table 3
Splitting of the excited energy levels of Er³⁺ and Yb³⁺ in KYW single crystal obtained after optical absorption at 6 K

	^{2S+1} L _J	Stark levels energy (cm ⁻¹)
(Yb)	² F _{5/2}	10 187, 10 490, 10 728
(Er)	⁴ I _{15/2}	0, 27, 62, 104, 137, 234, 289, 306
	⁴ I _{13/2}	6516, 6545, 6571, 6603, 6666, 6719, 6732
	⁴ I _{11/2}	10 188, 10 213, 10 229, 10 261, 10 284, 10 290
	⁴ I _{9/2}	1236, 12 392, 12 467, 12 497, 12 557
	⁴ F _{9/2}	15 193, 15 209, 15 332, 15 341, 15 368
	⁴ S _{3/2}	18 316, 18 380
	² H _{11/2}	19 041, 19 061, 19 132, 19 172, 19 207, 19 220
	⁴ F _{7/2}	20 430, 20 477, 20 501, 20 573
	⁴ F _{5/2}	22 112, 22 143, 22 182
	⁴ F _{3/2}	22 459, 22 552
	² H _{9/2}	24 491, 24 527, 24 545, 24 585, 24 613
	⁴ G _{11/2}	26 219, 26 235, 26 333, 26 390, 26 440, 26 462
⁴ G _{9/2}	27 274, 27 288, 27 328, 27 355, 27 370	

for the polarisation parallel to N_m principal optical direction. This agrees well with the results published by Pujol et al. [10], and Kuleshov et al. [13], where the samples were KYbW and KYW:Yb (5 at.%), respectively. The high absorption cross-section of ytterbium allows the excitation of erbium via energy transfer.

Fig. 6 shows the polarised optical absorption of KYW:Er,Yb in the 1425–1650 nm range at RT and the emission cross-section calculated by the Reciprocity method [14] for all three polarisations of the $^4I_{13/2} \rightarrow ^4I_{15/2}$ transition. The maximum absorption cross-section for the polarisation parallel to the N_m principal optical direction, which corresponds to the 1.534 μm (6519 cm^{-1}) signal, was about $2.7 \times 10^{-20} \text{ cm}^2$. This gave a maximum value of emission cross-section of $2.7 \times 10^{-20} \text{ cm}^2$, which is similar to the value published by Kuleshov et al. [15] and very similar to that of the excellent LaLiP₄O₁₂ laser material [16].

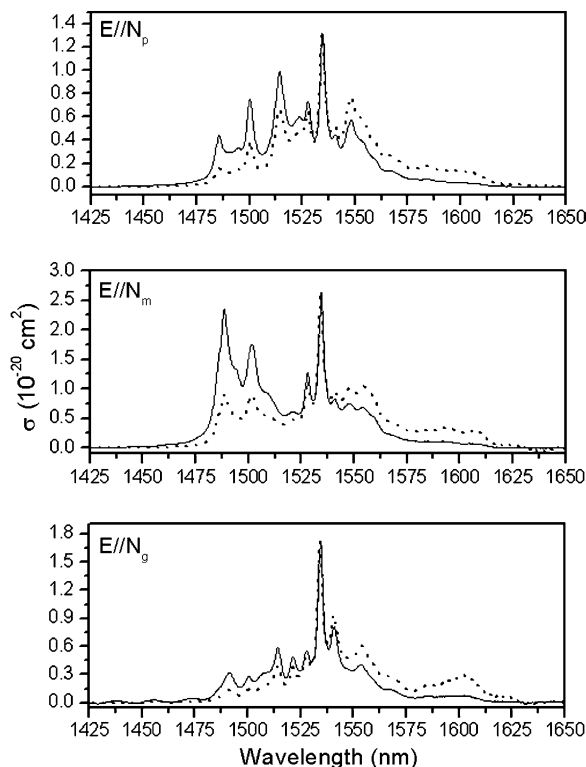


Fig. 6. Polarised optical absorption (solid line) ($^4I_{15/2} \rightarrow ^4I_{13/2}$ transition) and calculated emission (dotted line) cross-section of the 1.5 μm emission of erbium at RT.

Fig. 7 shows the polarised optical absorption of KYW:Er,Yb in the 350–1125 nm range at RT. Note the high absorption cross-section of the hypersensitive $^2H_{11/2}$ and $^4G_{11/2}$ levels and the anisotropy induced by the host.

We performed complementary studies of polarised optical absorption at 6 K to determine the Stark levels

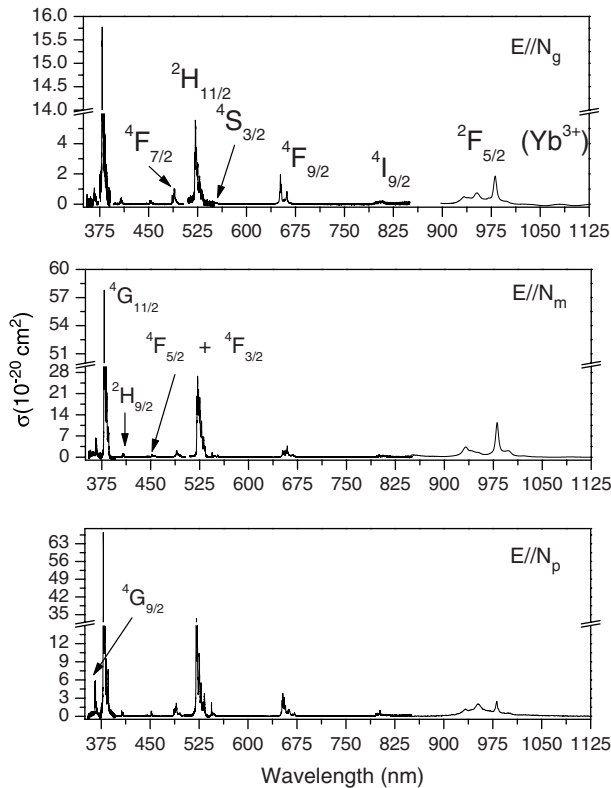


Fig. 7. Polarised optical absorption of Er^{3+} in the 350–1125 nm range at RT.

of all the possible excited energy levels caused by the elimination of the thermal population in the energy levels and the elimination of the thermal lattice vibrations. Fig. 8 shows the polarised optical absorption spectra performed at 6 K of the ${}^4\text{I}_{13/2}$ energy level in the 1450–1575 nm range. Fig. 9 shows the polarised optical absorption spectra performed at 6 K of all the excited energy levels of erbium in the 350–960 nm range. The crystal field splits these manifolds into $(2J + 1)/2$ sublevels. This is in agreement with the splitting expected by the crystalline field into the maximum number of Kramers levels (Stark levels or sublevels) due to the odd number of electrons of erbium and the low symmetry where erbium is located (C_2). In spite of the low temperature, some contributions of the optical absorption from the first Stark level of the ground state already exist. Table 3 shows the splitting of all the excited energy levels of erbium in KYW single crystals. In all cases, the excited energy levels show the number of expected sublevels. For the ${}^4\text{I}_{15/2} \rightarrow {}^4\text{I}_{13/2}$ transition, the number of sublevels was seven and the energy difference between the first sublevel, 1534.8 nm (6516 cm^{-1}) and the second sublevel, 1527.9 nm (6545 cm^{-1}) was 29 cm^{-1} . The energy difference between the first sublevel 1534.8 nm (6516 cm^{-1}) and the third sublevel, 1521.8 nm (6571 cm^{-1}) was 55 cm^{-1} . These energy differences will be used later to calculate the splitting of the ground state.

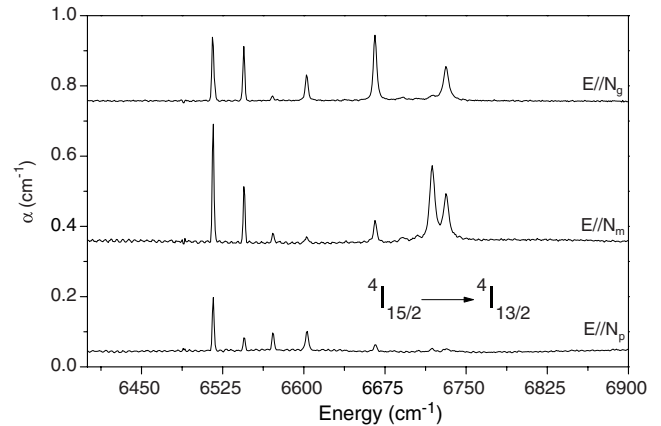


Fig. 8. Polarised optical absorption of Er^{3+} in the 1450–1575 nm range at 6 K.

3.3.2. Luminescence

We performed the luminescence experiments in terms of optical emission and lifetime measurements. The optical emission of erbium ions was carried out in the 1425–1650 nm range after pumping at 981 nm (overlap in energy between the ${}^4\text{I}_{11/2}$ and the ${}^2\text{F}_{5/2}$ levels of erbium and ytterbium, respectively) and 798 nm (${}^4\text{I}_{9/2}$ of erbium) at RT and 10 K.

Fig. 10 compares the experimental infrared emission (${}^4\text{I}_{13/2} \rightarrow {}^4\text{I}_{15/2}$ transition) after pumping at 981 nm with the spectrum calculated with the Reciprocity method by taking into account the average of the three absorption spectra for each polarisation. We rescaled the experimental spectrum to match the calculated spectra and compare its shape. As the figure shows, the two spectra are very similar, except at short wavelengths (higher energies), because the re-absorption effect is greater and the Reciprocity method does not consider this.

We performed systematic studies of photoluminescence of erbium at low temperature to determine the $1.5 \mu\text{m}$ (6667 cm^{-1}) emission channels and the splitting of the ground state of erbium. Fig. 11 shows the 10 K emission corresponding to the ${}^4\text{I}_{13/2} \rightarrow {}^4\text{I}_{15/2}$ transition under two pump wavelength, 981 and 798 nm. The number of sublevels expected due to the effect of the crystal field is eight. These clearly appear in the spectrum and are represented by (a) in the case of the 981 nm excitation. The energy values of these eight signals were 6518, 6490, 6456, 6412, 6381, 6283, 6227 and 6211 cm^{-1} . The spectrum also shows minor peaks, which are represented by (b) and (c) in the spectrum. These may be related to the transition from the second and third Stark levels of the ${}^4\text{I}_{13/2}$ (see inset of Fig. 11) to the Stark levels of the ground state. These peaks are displaced in accordance with the difference in energy between the first and second Stark levels ($\Delta E = 29 \text{ cm}^{-1}$) and the first and third Stark levels ($\Delta E = 55 \text{ cm}^{-1}$, see Table 3) of the excited ${}^4\text{I}_{13/2}$. From the energy positions corresponding to the ${}^4\text{I}_{13/2}$ sublevels (see Table 3) and by

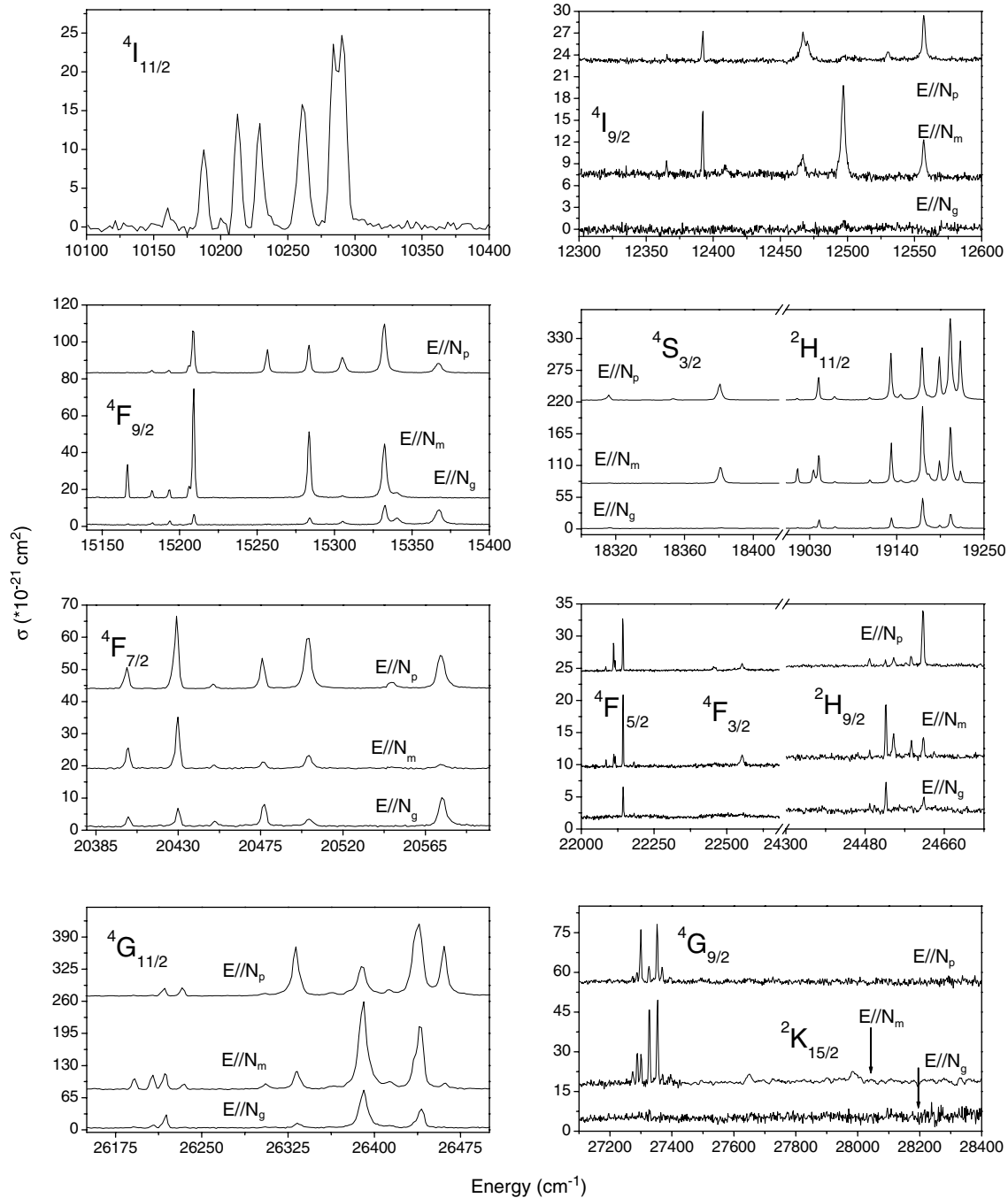


Fig. 9. Polarised optical absorption of Er^{3+} in the 350–960 nm range at 6 K.

subtracting the above-mentioned energy values of emission signals, we obtained the splitting of the ground state of erbium. The values were 0, 28, 62, 106, 137, 235, 291 and 307 cm^{-1} , which are very similar to those published in other tungstate hosts such as KGW [17], KYbW [18] and KErW [19].

In the case of the 798 nm excitation the values of the signals (represented by crosses in the spectrum) were 6518, 6491, 6456, 6414, 6381, 6284, 6229 and 6212 cm^{-1} . We calculated the energy position of the

Stark levels of the ground state. These values were 0, 27, 62, 104, 137, 234, 289 and 306 cm^{-1} , which coincided reasonably with those reported after 981 nm emission excitation. The most important difference between these spectra was the emission intensity and the resolution. Due to the sensitisation the intensity was higher with the 981 nm pump than with the 798 nm pump. In the spectrum we rescaled the signals to facilitate to the reader the assignment of the peaks. Otherwise, the resolution was better in the case of the 798 nm pump. We used

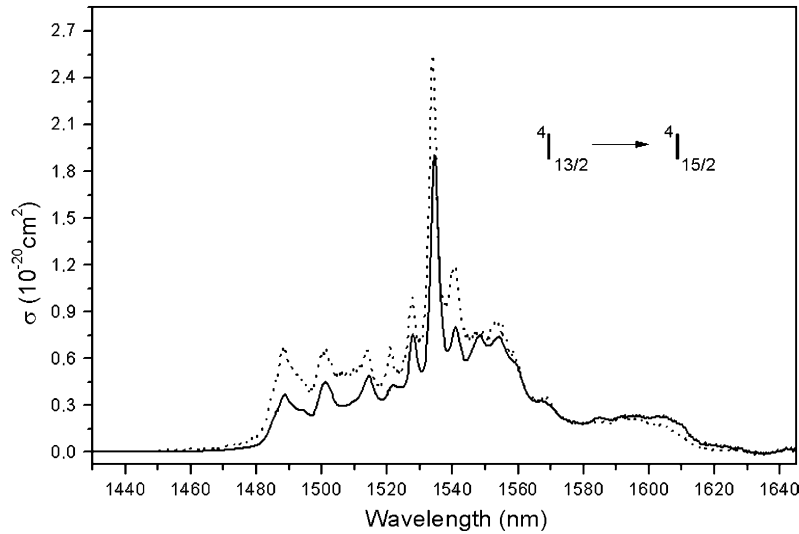


Fig. 10. Experimental (solid line) and calculated (dotted line) emission cross-sections of the 1.5 μm emission of erbium.

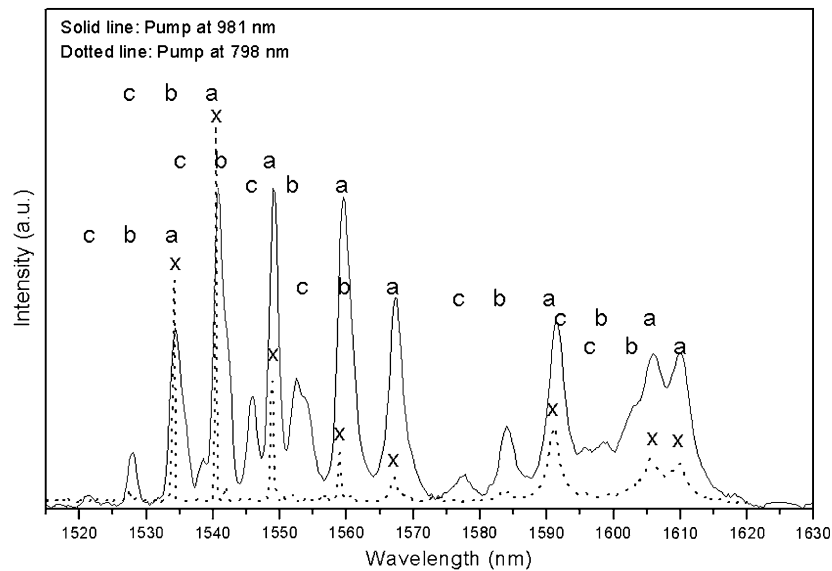


Fig. 11. Emission around 1.5 μm of erbium at 10 K after 981 and 798 nm pump. *Inset*: Schematic view of the 1.5 μm emission channels.

these results to schematise the emission channels around 1.5 μm (6667 cm^{-1}) and the energy position of all the Stark levels of the ground state in the inset of Fig. 11.

We also measured the lifetime at RT of the emitting level, $^4I_{13/2}$ for a dopant concentration of 0.5, 5% Er, Yb, respectively. This was 2160 μs .

4. Conclusions

We performed several optical studies of the TSSG-grown $\text{KY}(\text{WO}_4)_2$ single crystals, including the transparency window (from 350 to 5400 nm), the orientation of the principal optical axes (N_m was located at 18.5° with respect to the c crystallographic axis (clock-wise rotation)) and the dispersion of the refractive indices

along the three principal optical directions (the n_g ranged from 2.15 to 2.05 at 450 and 1500 nm, respectively, the n_m ranged from 2.10 to 2.01 and the n_p ranged from 2.05 to 1.97 at the same wavelengths).

We also performed the spectroscopic characterisation of erbium in this host after measuring the polarised optical absorption and the optical emission at RT and at low temperature in the 1425–1600 nm range at two pump wavelengths (981 and 798 nm). We also measured the lifetime of the observed emission at RT (2160 μs).

From the polarised RT optical absorption measurements, we calculated the stimulated emission cross-section by the Reciprocity method for the 1.5 μm emission ($2.7 \times 10^{-20}\text{ cm}^{-2}$ at 1534 nm for the $E||N_m$ direction).

From the 6 K polarised optical absorption measurements, we determined the energy position of the Stark level of each excited energy levels (see Table 3).

From the 6 K optical emission experiments, we found the energy position of the Stark levels of the ground level by means of the 1.5 μm emission (${}^4\text{I}_{13/2} \rightarrow {}^4\text{I}_{15/2}$) after pumping at 981 and 798 nm.

Acknowledgements

We gratefully acknowledge financial support from CICYT under Projects MAT2002-04603-C05-03, FIT-07000-2001-477, and FIT-07000-2002-461, and from CIRIT under Project 2001SGR00317.

References

- [1] S.V. Borisov, R.F. Kletsova, *Sov. Phys. Crystallogr.* 13 (1968) 420.
- [2] R. Guerin, P. Caillet, *C.R. Acad. Sci. Ser. C* 271 (1970) 815.
- [3] G. Wang, Z. Luo, *J. Cryst. Growth* 116 (1992) 505.
- [4] N. Manuilov, V. Nikolov, G. Gentsheva, P. Peshev, *J. Cryst. Growth* 169 (1996) 181.
- [5] G. Métrat, N. Muhlstein, A. Brenier, G. Boulon, *Opt. Mater.* 8 (1997) 75.
- [6] M.C. Pujol, R. Solé, V. Nikolov, Jna. Gavalda, J. Massons, C. Zaldo, M. Aguiló, F. Díaz, *J. Mater. Res.* 14 (1999) 3739.
- [7] R. Solé, V. Nikolov, A. Vilalta, J.J. Carvajal, J. Massons, Jna. Gavalda, M. Aguiló, F. Díaz, *J. Mater. Res.* 17 (2002) 563.
- [8] A.A. Kaminskii, A.F. Konstantinova, V.P. Orekhova, A.V. Butashin, R.F. Kletsova, A.A. Pavlyuk, *Crystallogr. Rep.* 46 (2001) 733.
- [9] M.C. Pujol, M. Rico, C. Zaldo, R. Solé, V. Nikolov, X. Solans, M. Aguiló, F. Díaz, *App. Phys. B* 68 (1999) 187.
- [10] M.C. Pujol, M.A. Bursukova, F. Güell, X. Mateos, R. Solé, Jna. Gavalda, M. Aguiló, J. Massons, F. Díaz, P. Klopp, U. Griebner, V. Petrov, *Phys. Rev. B* 65 (2002) 165121.
- [11] X. Mateos, R. Solé, Jna. Gavalda, M. Aguiló, J. Massons, F. Díaz, V. Petrov, U. Griebner, *Opt. Mat.*, in press.
- [12] L. Macalik, P.J. Deren, J. Hanuza, W. Strek, A.A. Demidovich, A.N. Kuzmin, *J. Mol. Struct.* 450 (1998) 179.
- [13] N.V. Kuleshov, A.A. Lagatsky, A.V. Podlipensky, V.P. Mikhailov, G. Huber, *Opt. Lett.* 22 (1997) 1317.
- [14] S.A. Payne, L.L. Chase, L.K. Smith, W.L. Kway, W.F. Krupke, *IEEE J. Quant. Electron.* 28 (1992) 2619.
- [15] N.V. Kuleshov, A.A. Lagatsky, A.V. Podlopiensky, V.P. Mikhailov, A.A. Kornienko, E.B. Dunina, S. Hartung, G. Huber, *J. Opt. Soc. Amer. B.* 15 (1998) 1205.
- [16] A.-F. Obaton, C. Parent, G. Le Flem, P. Thony, A. Brenier, G. Boulon, *J. Alloys Comput.* 300–301 (2000) 123.
- [17] X. Mateos, C. Pujol, F. Güell, M. Galán, R. Solé, Jna. Gavalda, M. Aguiló, J. Massons, F. Díaz, *IEEE J. Quant. Electron.* 40 (2004) 759.
- [18] X. Mateos, M.C. Pujol, F. Güell, R. Solé, Jna. Gavalda, M. Aguiló, F. Díaz, J. Massons, *Phys. Rev. B* 66 (2002) 214104.
- [19] A.A. Kaminskii, *Laser Crystals, their Physics and Properties*, second ed. Springer Ser. Opt. Sci., vol. 14, Springer, Berlin, 1990.